Deposition of WC on TiO_2 nanosheets with exposed (001) facets for photocatalytic degradation

Y. Q. Dong [a], Y. C. Zhang [a], B. H. Ren [a], S. N. Liu [a], Y. Li [a], Y. Sun [a, b,*]
[a]*School of Mechanical Engineering, Chengdu University, Chengdu, 610106, China*
[b]*Sichuan Province Engineering Technology Research Center of Powder Metallurgy, Chengdu, 610106, China.*

Anatase TiO_2 nanosheets with exposed (001) facets were prepared by a hydrothermal method under HF condition. Then, commercial WC particles were deposited on TiO_2 nanosheets by physical mixing method. The prepared samples were characterized by X-ray diffraction (XRD), scanning electron microscopy (SEM), transmission electron microscopy (TEM), UV-vis diffuse reflectance spectroscopy (DRS), X-ray photoelectron spectroscopy and nitrogen adsorption-desorption isotherms. To investigate the effect of WC loading on the photocatalytic performance, the degradation of Rhodamine B (RhB) dye was conducted under simulated light. The results indicated that the WC/TiO_2 exhibited higher photocatalytic activity than pure TiO_2 catalyst. When the WC loading was 10 wt%, the degradation efficiency reached 90.2% within 60 min. The enhanced photocatalytic performance may be attributed to the introduction of WC particles which could react as an electron trap and promote the separation of photogenerated electron-hole pairs of TiO_2. Meanwhile, the trapping experiment confirmed that superoxide radical ($\cdot O_2^-$) and hole (h^+) played leading roles in the degradation of RhB.

(Received January 28, 2023; Accepted April 13, 2023)

Keywords: TiO_2 nanosheets, WC, Rhodamine B, Photocatalysis

1. Introduction

With the rapid development of economy, a large number of organic dyes has been used in various technical applications, including the process of textiles, paper, leather, plastics, paints and coatings [1]. Consequently, the wastewater from the industries caused environmental pollution and human health problems [2]. In the past years, photocatalysis has been proposed as a promising approach for wastewater treatment using different types of semiconductor materials such as TiO_2, WO_3, $BiWO_6$, g-C_3N_4, and ZnO [3-7]. Among these photocatalysts, TiO_2 has been widely investigated due to its high oxidation, photostability, non-toxicity and low cost [8,9]. However, the large bandgap (3.2 eV) of TiO_2 resulting in the poor absorption of solar light limits its photocatalytic application [10]. Therefore, it is particularly important to extend the optical absorption range of TiO_2 to visible region [11]. Moreover, the fast recombination of photogenerated electron-hole pairs also restricts the photocatalytic performance of TiO_2 [12].

Recently, anatase TiO_2 nanosheets with higher surface energy of (001) facets have been extensively studied in photocatalysis. Both theoretical and experimental studies show that the anatase TiO_2 crystals with exposed (001) facets possess higher photocatalytic activity compared to TiO_2 with other facets [13-14]. Han et al. [15] have synthesized anatase TiO_2 with exposed (001) facets by hydrothermal method using HF as a morphology controlling agent. Furthermore, the single-crystalline structure of TiO_2 with a low density of defects can also suppress the recombination of photogenerated electron-hole pairs, leading to the enhancement of photocatalytic

* Corresponding author: sunyan@cdu.edu.cn
https://doi.org/10.15251/DJNB.2023.182.523

efficiency [16]. Besides, noble metals loading (Au, Ag, Pt) [17-19] on the TiO_2 surface can be considered as an effective way to improve the photocatalytic efficiency. The loading of noble metals can act as an electron trap which hinders the recombination of electron-hole pairs and enhances the charge transfer. However, the capture of electrons by noble metals is quite expensive that limits the large-scale application of noble metals. Thus, replacing rare noble metal-based catalysts with low-cost is crucial and becomes a hot research issue.

Tungsten carbide (WC) with appropriate work function (5.0 eV), excellent stability and abundant active sites [20], is proved to be a low-cost cocatalyst that could substitute noble metals in the fields of electrocatalysis [21-23]. To the best of our knowledge, there is no report on the application of tungsten carbide for photocatalytic degradation. Here, sheet-like anatase TiO_2 with exposed high activity (001) surface were successfully synthesized via hydrothermal method and commercial WC particles were deposited on TiO_2 nanosheets by the physical mixing method to reduce the recombination rate of electron-hole pairs. The effect of WC loading of in WC/TiO_2 photocatalysts on the photocatalytic degradation of RhB dye was discussed. This work provides a new route to replace noble metals with non-noble metals in the photocatalysis.

2. Experimental

2.1 Synthesis of catalysts

The TiO_2 nanosheets were prepared by a hydrothermal method [24]. Typically, 3 mL of hydrofluoric acid (HF, ≥ 40.0%) was added dropwise into 25 mL tetrabutyl titanate with stirring. Then the suspension was transferred to a 100 mL Teflon-lined autoclave and heated at 180 ℃ for 24 h. After cooling down to room temperature, the final product was washed with distilled water for several times and dried at 80 ℃ overnight.

The WC/TiO_2 catalysts were synthesized via the physical mixing method. Briefly, 300 mg of TiO_2 powder and a certain amount (10 wt%, 25% wt%) of commercial WC powder (Chengdu Chron Chemicals Co., Ltd) were added into 30 mL ethanol, followed by ultrasonic treatment for 30 min and stirring for 1 h. Finally, the samples were obtained by drying at 70 ℃ overnight.

2.2. Characterization

The crystal structure of samples was characterized by X-ray diffraction (DX-2700B) with Cu-Kα radiation ranged from 20° to 60°. The microstructure and morphology characterizations of photocatalyst were performed by scanning electron microscopy (Hitachi S4800) and transmission electronic microscopy (Talos F200S). Ultraviolet-visible diffuse reflectance spectra were obtained with a TU-1901 diffuse reflectance spectrometer using $BaSO_4$ as the reference. The valence band of samples were determined by X-ray photoelectron spectroscopy (Escalab Xi+). The specific surface area was measured by the Brunauer-Emmett- Teller (BET) method using V-sorb 2800p apparatus.

2.3. Photocatalytic experiment

The photocatalytic activity of the samples was evaluated by the degradation of RhB dye under irradiation. The light source was a 500 W Xenon lamp with a cut-off filter of AM 1.5 (100 mW/cm^2). In a typical procedure, 100 mg of photocatalyst was dispersed in 100 ml RhB solution (10 mg/L). The suspension was stirred in the dark for 30 min to achieve the adsorption-desorption equilibrium. During the photocatalytic degradation, the suspension was taken from the reactor at a certain time interval and centrifuged. The concentration of RhB was measured by the UV-vis spectrophotometer at the wavelength of 554 nm.

The trapping experiments were carried out by adding 1,4-benzoquinone (BQ, 1 mM), isopropanol (IPA, 20 mM) and triethanolamine (TEOA, 20 mM) into RhB solution to capture superoxide radicals ($\cdot O_2^-$), hydroxyl radicals ($\cdot OH$) and holes (h^+), respectively.

3. Results and discussion

Fig. 1 shows the XRD patterns of WC, TiO_2 and WC/TiO_2 samples with different WC loadings. In the TiO_2 pattern, the diffraction peaks at 25.3°, 37.8°, 48.0° and 55.3° can be indexed to (101), (004), (200) and (211) planes, which matches well with the anatase TiO_2 (JCPDS#

21-1272). The main peaks at 31.5°, 35.6° and 48.3° for WC (JCPDS# 51-0939) are assigned to the (001), (100) and (101) planes, respectively. For the WC/TiO_2 catalysts, the characteristic peaks of WC and TiO_2 can be observed in the XRD pattern and no other peaks are detected, suggesting the successful synthesis of WC/TiO_2 catalyst. In addition, the peak intensity of WC in WC/TiO_2 sample becomes stronger with the increase of WC amount.

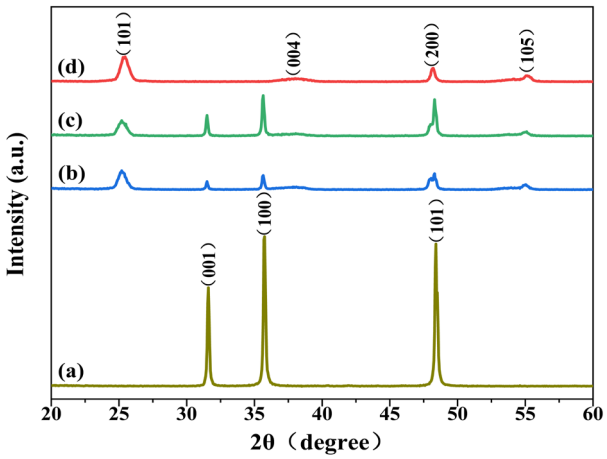

Fig. 1. XRD patterns of (a) WC, (b) 10 wt% WC/TiO_2, (c) 25 wt% WC/TiO_2 and (d) TiO_2.

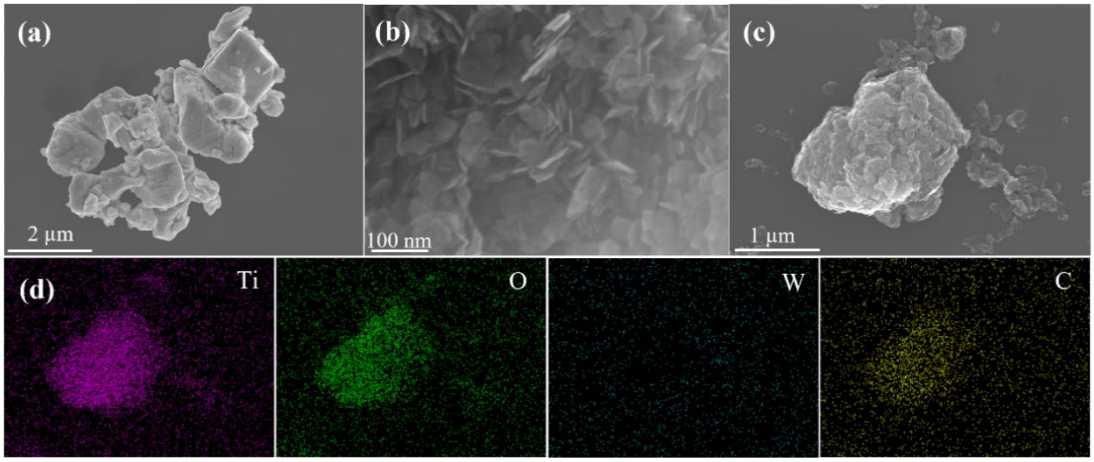

Fig. 2. SEM images of (a) WC, (b) TiO_2 and (c) 10 wt% WC/TiO_2; (d) the elemental mapping images.

The morphology of WC, TiO_2 and 10 wt% WC/TiO_2 is shown in Fig. 2. It is clear that the commercial WC powder displays bulk morphology which is composed of aggregated particles with the size of several micrometers (Fig. 2a). Fig. 2b exhibits typical anatase TiO_2 nanosheets structure prepared by a hydrothermal method under HF condition [24] and the synthesized TiO_2 nanosheets are in good uniformity. As shown in Fig. 2c, ultrathin TiO_2 nanosheets are successfully covered on the surface of WC particles through physical mixing. The elemental mapping images of 10 wt% WC/TiO_2 (Fig. 2d) reveal the existence of Ti, O, W and C elements in WC/TiO_2 photocatalyst, which further confirms the deposition of WC particles in the hybrid sample.

The microstructural details of TiO_2 nanosheets and 10 wt% WC/TiO_2 were further analyzed by TEM and HRTEM. Fig. 3a shows that the TiO_2 is in a rectangular shape with an average side length of 40-60 nm. In Fig. 3b, both WC particles and TiO_2 nanosheets can be clearly observed in the 10 wt% WC/TiO_2 sample. The HRTEM image of 10 wt% WC/TiO_2 is presented in Fig. 3c. The crystal lattice spacing of 0.235 nm and 0.35 nm corresponds to the (001) and (101) crystal planes of anatase TiO_2 [25], respectively. The lattice fringes of 0.19 nm can be ascribed to

(101) plane of WC [26]. In addition, the higher specific surface area of TiO_2 nanosheets is measured as 110.52 m^2g^{-1} while that of 10 wt% WC/TiO_2 decreases to 94.12 m^2g^{-1} due to the loading of WC microparticles.

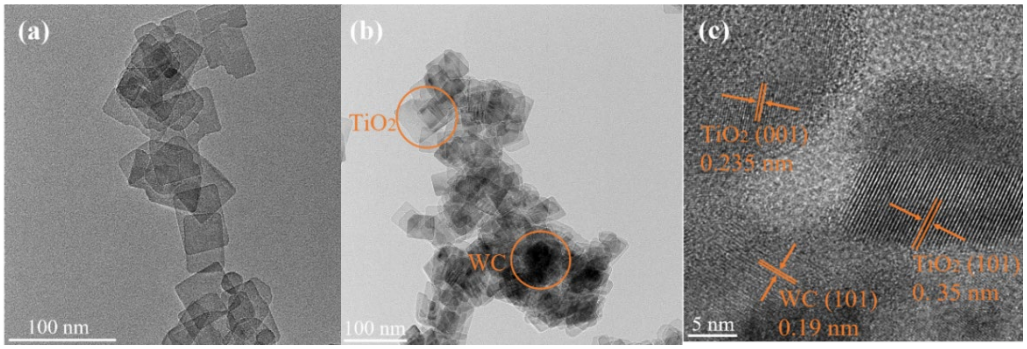

Fig. 3. TEM images of (a) TiO_2, (b) 10 wt% WC/TiO_2 and (c) HRTEM image of 10 wt% WC/TiO_2.

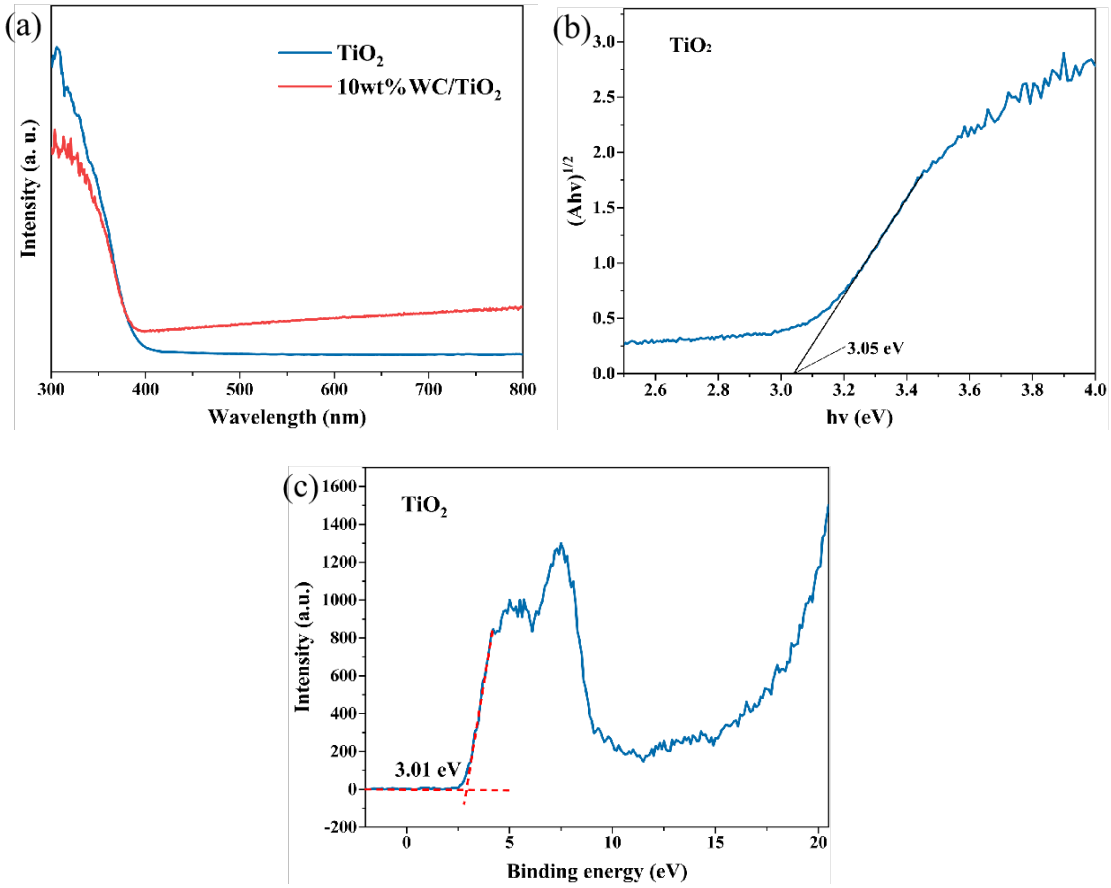

Fig. 4. (a) UV-vis DRS spectra; (b) the bandgap of TiO_2; (c) the XPS valence band spectrum of TiO_2.

The optical properties of TiO_2 and 10 wt% WC/TiO_2 are investigated by DRS. As shown in Fig. 4a, the absorption edge of TiO_2 is shorter than 400 nm owing to the intrinsic bandgap absorption of anatase TiO_2. After the loading of WC, the absorption edge of WC/TiO_2 sample obviously extends to the visible light range. The bandgap of TiO_2 is determined as 3.05 eV (Fig. 4b)

according to equation [27]:

$$\alpha hv = A(hv - E_g)^{n/2}$$

where α is the absorption, h is the Planck constant, v is the frequency, E_g is the forbidden band width of the semiconductor material, and A is the absorption coefficient. Meanwhile, the XPS valence band (VB) value of TiO_2 is estimated to be 3.01 eV (Fig.4c) and the final VB position of TiO_2 is calculated as 3.17 eV by the following formula [28]:

$$E_{NHE} = \phi - E_{VL} \quad (4)$$

where E_{NHE} is potential of normal hydrogen electrode, ϕ is electron work function of the instrument (4.6 eV) and E_{VL} is the potential of vacuum level, respectively. Based on the results above, the conduction band (CB) value of 0.12 eV can be obtained.

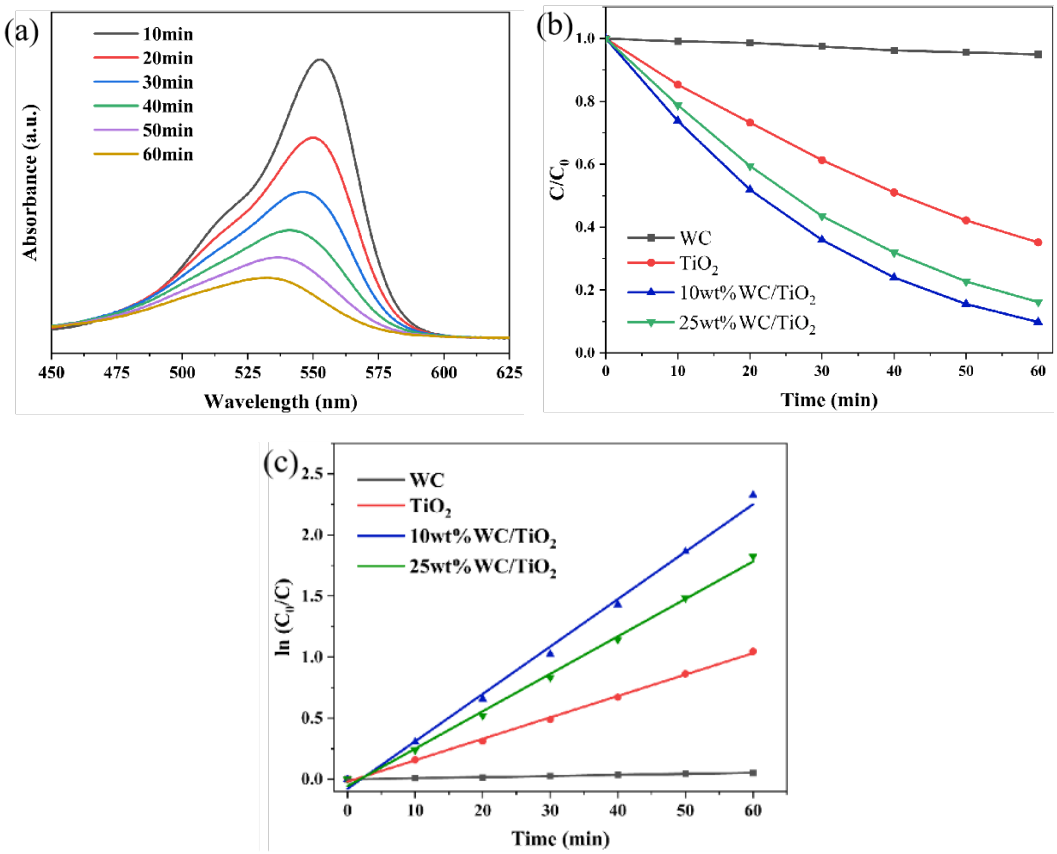

Fig. 5. (a) UV-vis absorption spectra of RhB at different irradiation times in the presence of 10 wt% WC/TiO_2; (b) the comparison of photocatalytic degradation and (c) the first-order kinetics curves.

The photocatalytic performance of various catalysts is evaluated by RhB degradation. Fig. 5a shows the *UV*-vis absorption spectra of RhB solution tested at different irradiation times with 10 wt% WC/TiO_2 catalyst. It is found that the absorbance of RhB solution weakens gradually with increasing irradiation time, indicating the removal of RhB dye. Fig. 5b compares the photocatalytic activity of various catalysts. The degradation efficiency of WC and TiO_2 is only 5.0% and 64.9% within 60 min. With 10 wt% loading of WC, nearly 90.2% of RhB dye has been degraded. However, with further increase of WC to 25 wt%, the degradation efficiency of WC/TiO_2 decreases to 83.9%. Therefore, there is an optimum value of 10 wt% in the WC/TiO_2 catalyst for the photocatalytic degradation. The enhancement of photocatalytic activity is ascribed

to the presence of WC that could promote charge separation and reduce the recombination of electron-hole pairs. Fig. 5c shows the degradation dynamic curves over all samples. It is obvious that the degradation rate of all catalysts conforms to the pseudo-first order kinetic model. The rate constant of 10 wt% WC/TiO_2 sample is 0.03883 min^{-1}, which is 1.21 times higher than that of pure TiO_2 (0.01754 min^{-1}).

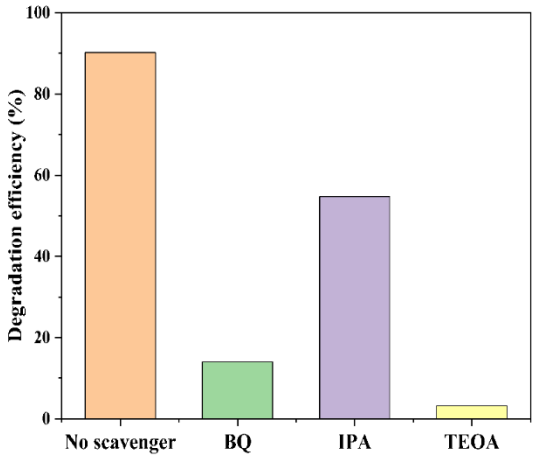

Fig. 6. Reactive species trapping experiment of 10 wt% WC/TiO_2.

The trapping experiment of 10 wt% WC/TiO_2 catalyst was performed to detect the main active species during the photocatalytic degradation process. As shown in Fig. 6, after the addition of BQ, TEOA and IPA, the photocatalytic degradation efficiency decreases to 14.0%, 3.2% and 56.8%, respectively. It can be inferred that the degradation of RhB is mainly driven by $\cdot O_2^-$ and h^+ species.

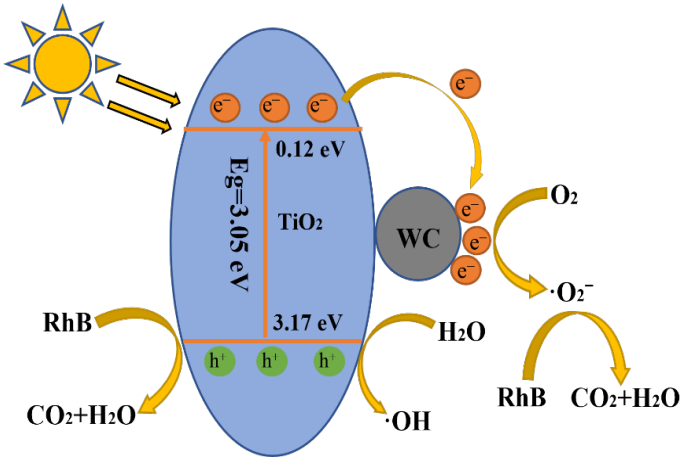

Fig. 7. Schematic diagram of the charge transfer mechanism for WC/TiO_2 photocatalyst.

On the basis of the results above, the mechanism of photocatalytic degradation is proposed in Fig. 7. Under light illumination, the electrons in VB of TiO_2 are excited and transfer to CB, while the holes are left in the VB. As the Fermi level of WC (0.5 eV) is lower than the TiO_2 [29], the photogenerated electrons excited to CB of TiO_2 could overcome Schottky barrier and easily move to WC particles. In this process, WC as an electron trap could capture and store the photogenerated electrons, which significantly facilitates the separation of charge carriers. Thus, the electrons aggregated on the WC could react with absorbed O_2 to produce $\cdot O_2^-$. On the other hand, a

large number of h^+ remained on VB of TiO_2 can directly oxidize organic dye molecule, accelerating the decomposition of RhB.

4. Conclusion

In summary, commercial WC particles were successfully deposited on TiO_2 nanosheets with exposed (001) facets by the physical mixing method. The WC could react as an electron trap and promote the separation of the photogenerated charge carriers. Therefore, the photocatalytic activity could be significantly enhanced by loading WC particles. The highest photocatalytic efficiency reached 90.2% within 60 min when the loading of WC was 10 wt%. The trapping test indicated that h^+ and $\cdot O_2^-$ played main roles in the decomposition of RhB dye.

Acknowledgments

This research was supported by the Science and Technology Planning Project of Longquanyi, Chengdu (No. LQXKJ-KJXM-2022-04).

References

[1] M. Chin, C. Cisneros, S. M. Araiza, K. M. Vargas, K. M. Ishihara, F. Y. Tian. RSC. Adv. 8, 26987 (2018); https://doi.org/10.1039/c8ra03459a.
[2] C. A. Martínez-Huitle, E. Brillas, Appl. Catal. B-Environ. 87, 105 (2008); https://doi.org/10.1016/j.apcatb.2008.09.017.
[3] Y. Sun, S. Xu, J. Y. Zeng, S. S. Yang, Q. R. Zhao, Y. Yang, Q. Zhao, G. X. Wang, Dig. J. Nanomater. Bios. 16(1), 239 (2021);
[4] Q. R. Zhao, S. Y. Chen, B. H. Ren, S. N. Liu, Y. C. Zhang, X. Luo, W. Feng, Y. Sun, Opt. Mater. 135, 113266 (2023); https://doi.org/10.1016/j.optmat.2022.113266.
[5] J. Wang, X. D. Zhu, F. Q. Qin, Y. X. Wang, Y. Sun, W. Feng, Mater. Lett. 314, 13182 (2022); https://doi.org/10.1016/j.matlet.2022.131892.
[6] Y. Yang, D. Y. Wang, Y. C. Zhang, S. Y. Chen, Y. Sun, Dig. J. Nanomater. Bios. 17(4), 1491 (2022); https://doi.org/10.15251/DJNB.2022.174.1491.
[7] X. B. Yang, Z. D. Wen, Z. L. Wu, X.T. Luo, Inorg. Chem. Front. 5, 687 (2018); https://doi.org/10.1039/c7qi00752c.
[8] L. G. Xiao, Z. L. Yang, H. R. Zhu, G. Yan, Inorg. Chem. Commun. 146, 110167 (2022); https://doi.org/10.1016/j.inoche.2022.110167.
[9] M, Stucchi, C. L. Bianchi, C. Argirusis, V. Pifferi, B. Neppolian, G. Cerrato, D. C. Boffito, Ultrason. Sonochem. 40, 282 (2018); http://dx.doi.org/10.1016/j.ultsonch.2017.07.016.
[10] K. Alamelu, B. M. J. Ali, J. Environ. Chem. Eng. 6(5), 5720 (2018); https://doi.org/10.1016/j.jece.2018.08.042.
[11] L. Yang, M. G. Gao, B. Dai, X. H. Guo, Z. Y. Liu, B. H. Peng, Appl. Surf. Sci. 386, 337 (2016); http://dx.doi.org/10.1016/j.apsusc.2016.06.043.
[12] W. Y. Choi, A. Termin, M. R. Hoffmann, J. Phys. Chem. 98, 13669 (1994); http://dx.doi.org/10.1021/j100102a038.
[13] J. G. Yu, J. J. Fan, K. L. Lv, Nanoscale 2(10), 2144 (2010); http://dx.doi.org/10.1039/c0nr00427h.
[14] H. G. Yang, C. H. Sun, S. Z. Qian, J. Zou, G. Liu, S. C. Smith, H. M. Cheng, G. Q. Lu, Nature

453, 638 (2008); http://dx.doi.org/10.1038/nature06964.
[15] X. G. Han, Q. Kuang, M. S. Jin, Z. X. Xie, L. S. Zheng, J. Am. Chem. Soc. 131(9), 3152 (2009); http://dx.doi.org/10.1021/ja8092373.
[16] X. L. Wang, H. L. He, Y. Chen, J. Q. Zhao, X. Y. Zhang, Appl. Sure. Sci. 258, 5863 (2012); http://dx.doi.org/10.1016/j.apsusc.2012.02.117.
[17] Y. Wen, B. T. Liu, W. Zeng, Y. H. Wang, Nanoscale 5, 9739 (2013); http://dx.doi.org/10.1039/C3NR03024E.
[18] M. K. Seery, R. George, P. Floris, S. C. Pillai, J. Photoch. Photobio. A. 189(2-3), 258 (2007); http://dx.doi.org/10.1016/j.jphotochem.2007.02.010.
[19] Y. Sun, Y. Gao, J. Y. Zeng, J. Guo, H. Wang, Mater. Lett. 279, 128506 (2020); https://doi.org/10.1016/j.matlet.2020.128506.
[20] Y. K. Huang, S. W. Kou, X. T. Zhang, L. Wang, D. J. Zhang, Ceram. Int. 47(14), 20626 (2021); https://doi.org/10.1016/j.ceramint.2021.04.072.
[21] J. S. Jang, D. J. Ham, N. Lakshminarasimhan, W. Y. Choi, J. S. Lee, Appl. Catal. A-Gen. 346, 149 (2008); http://dx.doi.org/10.1016/j.apcata.2008.05.020.
[22] Y. X. Pan, H. Q. Zhuang, H. Ma, J. Cheng, J. Song, Chem. Eng. Sci. 194, 71 (2018); https://doi.org/10.1016/j.ces.2018.01.022.
[23] Y. X. Pan, T. H. Zhou, J. Y. Han, J. D. Hong, Y. B. Wang. W. Zhang, R. Xu, Catal. Sci. Technol. 6, 2206 (2016); http://dx.doi.org/10.1039/c5cy01634g.
[24] S. L. Chen, D. Li, Y. X. Liu, W. X. Huang, J. Catal. 341, 126 (2016); http://dx.doi.org/10.1016/j.jcat.2016.06.016.
[25] Y. C. Wu, Z. M. Liu, Y. R. Li, J. T. Chen, X. X. Zhu, P. Na, Chinese J. Catal. 40, 60 (2019); https://doi.org/10.1016/S1872-2067(18)63170-5.
[26] C. J. Ren, W. J. Li, S. N. Gu, X. T. Liu, X. Y. Li, H. X. Fan, K. Han, X. H. Ma, Appl. Mater. Today 20, 100731 (2020); https://doi.org/10.1016/j.apmt.2020.100731.
[27] W. H. Zhang, Z. Y. Bian, X. Xin, L. Wang, X. L. Geng, H. Wang, Chemosphere 262, 127955 (2021); https://doi.org/10.1016/j.chemosphere.2020.127955.
[28] Y. Lu, K. Zhao, Y. H. Zhao, S. Y. Zhu, X. Yuan, M. X. Huo, Y. Zhang, Y. Qiu, Colloid. Surface. A. 481, 252 (2015); http://dx.doi.org/10.1016/j.colsurfa.2015.05.037.
[29] S. L. Wang, Y. Zhu, X. Luo, Y. Huang, J. W. Chai, T. I. Wong, G. Q. Xu, Adv. Funct. Mater. 28(11), 1705357 (2018); http://dx.doi.org/10.1002/adfm.201705357.